HHS Public Access

Author manuscript

Cell Rep. Author manuscript; available in PMC 2016 February 04.

Published in final edited form as:

Cell Rep. 2015 August 4; 12(5): 760–773. doi:10.1016/j.celrep.2015.06.074.

miR-302 Is Required for Timing of Neural Differentiation, Neural Tube Closure, and Embryonic Viability

Ronald J. Parchem[1,2], **Nicole Moore**[1,2], **Jennifer L. Fish**[3], **Jacqueline G. Parchem**[4], **Tarcio T. Braga**[1,2], **Archana Shenoy**[1,2], **Michael C. Oldham**[1,5], **John L.R. Rubenstein**[6], **Richard A. Schneider**[3], and **Robert Blelloch**[1,2,*]

[1]The Eli and Edythe Broad Center of Regeneration Medicine and Stem Cell Research, Center for Reproductive Sciences, University of California, San Francisco, San Francisco, CA 94143, USA

[2]Department of Urology, University of California, San Francisco, San Francisco, CA 94143, USA

[3]Department of Orthopaedic Surgery, University of California, San Francisco, San Francisco, CA 94143, USA

[4]Department of Obstetrics, Gynecology & Reproductive Sciences, University of California, San Francisco, San Francisco, CA 94143, USA

[5]Department of Neurology, University of California, San Francisco, San Francisco, CA 94143, USA

[6]Department of Psychiatry, University of California, San Francisco, San Francisco, CA 94143, USA

SUMMARY

The evolutionarily conserved miR-302 family of microRNAs is expressed during early mammalian embryonic development. Here, we report that deletion of miR-302a-d in mice results in a fully penetrant late embryonic lethal phenotype. Knockout embryos have an anterior neural tube closure defect associated with a thickened neuroepithelium. The neuroepithelium shows increased progenitor proliferation, decreased cell death, and precocious neuronal differentiation. mRNA profiling at multiple time points during neurulation uncovers a complex pattern of changing targets over time. Overexpression of one of these targets, *Fgf15*, in the neuroepithelium of the chick embryo induces precocious neuronal differentiation. Compound mutants between

*Correspondence: robert.blelloch@ucsf.edu.

ACCESSION NUMBERS

The expression array data reported in this paper have been deposited to the NCBI GEO and are available under accession number GEO: GSE62396.

SUPPLEMENTAL INFORMATION

Supplemental Information includes Supplemental Experimental Procedures and six figures and can be found with this article online at http://dx.doi.org/10.1016/j.celrep.2015.06.074.

AUTHOR CONTRIBUTIONS

R.J.P. contributed to Figures 1, 2, 3, 4, 5, 6, and 7 and Figures S1–S6. N.M. contributed to Figures 1, 2, 3, 4, 5, 6, and 7 and Figures S1–S6. J.L.F. contributed to Figures 6C–6E. J.G.P. contributed to Figure 4D and Figures S4–S6. T.T.B. contributed to Figure 6B. A.S. and M.C.O contributed to Figure 5A. J.L.R.R. and R.A.S. contributed with data interpretation and experimental design. R.J.P. and R.B. wrote the manuscript.

mir-302 and the related *mir-290* locus have a synthetic lethal phenotype prior to neurulation. Our results show that *mir-302* helps regulate neurulation by suppressing neural progenitor expansion and precocious differentiation. Furthermore, these results uncover redundant roles for *mir-290* and *mir-302* early in development.

Graphical Abstract

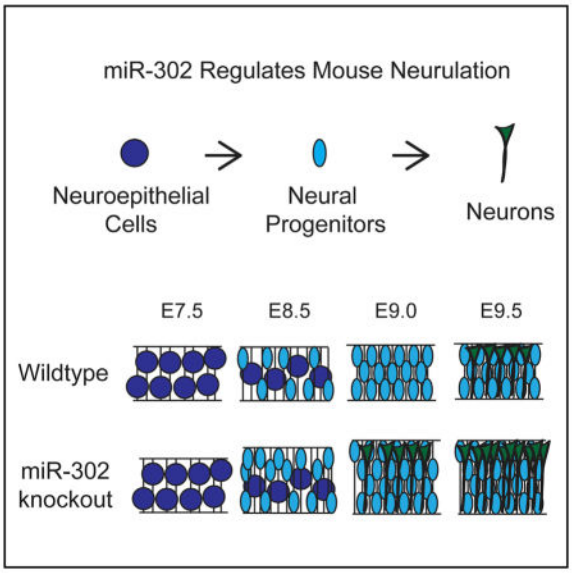

INTRODUCTION

In non-fish vertebrates, neurulation is the morphogenetic process whereby the neural plate folds into the neural tube. In humans, failure to complete this event leads to neural tube closure defects, which occur in approximately 1 in 1,000 births. The genetic underpinnings of neural tube closure are complex and involve different cellular processes (Copp and Greene, 2010). Proliferation of neuroepithelial cells prior to closure increases the number of cells within the neural tube. Neuroepithelial cells then give rise to progenitors that can either continue to undergo mitosis or generate neural cells, starting with neurogenesis followed later by gliogenesis. Proper timing of the transition from neural plate stage neuroepithelial cells to neural tube progenitors that subsequently generate neurons is carefully orchestrated during the neurulation morphogenetic program. The molecular mechanisms regulating the temporal sequence of these processes are poorly understood. Here, we provide evidence that microRNAs (miRNAs) help coordinate this differentiation program.

MiRNAs are small, ~21 nt, single-stranded RNAs that negatively regulate the stability and translation of mRNA transcripts (Bartel, 2009). In general, miRNAs target sequences within the 3′UTRs of mRNA transcripts that are highly complementary to the miRNA seed sequence (nucleotides 2–8) and have imperfect complementarity outside of the seed region. Because of the degenerate nature of miRNA:mRNA interactions, a single miRNA may have many mRNA targets. Surprisingly, although loss of all miRNAs results in early embryonic lethality (Bernstein et al., 2003; Wang et al., 2007), deletion of individual miRNAs or entire

clusters in mice has resulted in incompletely penetrant embryonic phenotypes or defects postnatally; indeed, there have been no confirmed examples of an absolute requirement for an individual miRNA locus in embryonic development (Vidigal and Ventura, 2015; Park et al., 2010; Ebert and Sharp, 2012). These findings in mice, as well as in nematodes and zebrafish, have led to the view that miRNAs fine-tune gene expression rather than play central roles in development (Reinhart et al., 2000; Giraldez et al., 2005; Ebert and Sharp, 2012; Abbott et al., 2005; Alvarez-Saavedra and Horvitz, 2010; Miska et al., 2007).

miRNAs are processed from longer RNAs, typically from long non-coding RNAs or introns within coding RNAs (Bartel, 2009). Often, multiple miRNAs are encoded by a single transcript called a miRNA cluster. miRNAs arising from two clusters, *mir-302/367 (mir-302)* and *mir-290/295 (mir-290)*, are highly enriched in pluripotent stem cells and early embryos in mice, as are their orthologs in humans (Houbaviy et al., 2003; Suh et al., 2004; Stadler et al., 2010; Jouneau et al., 2012). These two clusters encode multiple miRNAs that share a common seed sequence, which can be shifted because of alternative processing (e.g., miR-302c) and thus together form a miRNA family (Houbaviy et al., 2005; Seong et al., 2014). The earliest role identified for this family was in the regulation of the unique cell-cycle structure of embryonic stem cells (ESCs), for which they were named the ESCC, or ESC cell cycle regulating, miRNAs (Wang et al., 2008). Since then, multiple functions have been uncovered for these miRNAs, including cell-cycle regulation, inhibition of ESC differentiation, inhibition of apoptosis, and promotion of somatic cell reprogramming (reviewed in Greve et al., 2013).

In vitro, the ESCC miRNAs can function interchangeably. However, in vitro, the two clusters encoding these miRNAs have both overlapping and divergent patterns of expression. Ubiquitously expressed when the zygotic genetic program is initially activated, *mir-290* expression later becomes restricted to extra-embryonic structures such as the placenta and yolk sac (Parchem et al., 2014; Tang et al., 2007). Conversely, *mir-302* expression begins after implantation, specifically in the embryo proper and is co-expressed with *mir-290* until embryonic day (E) 7.0, at which point *mir-290* is downregulated while *mir-302* expression persists (Parchem et al., 2014; Houbaviy et al., 2005; Card et al., 2008; Tang et al., 2007). The genetic deletion of *mir-290* results in partially penetrant embryonic lethality and female sterility (Medeiros et al., 2011); the genetic deletion of *mir-302* has not been previously described.

Here, by producing and evaluating a *mir-302a-d*-specific knockout model, we identify an essential miRNA in mammalian development. Deletion of *mir-302a-d* led to increased neural progenitor proliferation early, decreased apoptosis late, precocious neural differentiation during neurulation, and a failure in neural tube closure. The atypical fibroblast growth factor family member, *Fgf15*, was found to be a direct target of miR-302, and its overexpression in chick neural ectoderm induced precocious neuronal differentiation, recapitulating one of the multiple defects seen in *mir-302* knockouts. Deletion of the *mir-290* cluster along with *mir-302a-d* resulted in early embryonic lethality, demonstrating redundancy between these two miRNA clusters. Together, these results show that the ESCC miRNAs are required for mammalian embryonic development, with *mir-302* in particular functioning as a regulator of neural development.

RESULTS

mir-302 Cluster Expression in Early Embryos

Previously, the expression of the *mir-302* cluster was evaluated through gastrulation until E8.0 using a knockin *mir-302-eGFP* reporter (Figure 1A) (Parchem et al., 2014). The reporter was activated at E5.5 and remained active throughout the embryo until E8.0. Here we analyzed expression post-gastrulation. By E8.5, the reporter was largely localized to the anterior neural plate, where it continued to be expressed during formation of the hind, mid, and forebrain structures (E9.5) (Figure 1A). However, reporter activity was largely absent by E10.5 (data not shown). Transverse sections of E9.5 cephalic regions showed dim GFP expression throughout, with higher expression in the ventral floor plate and notochord (Figure S1). Consistent with reporter activity, qRT-PCR showed decreasing levels of mature miR-302b,c and miR-367 from E7.5 to E9.5 (Figure 1B). The miRNAs were undetectable at E11.5. Together, these expression data suggest an initial broad role for miR-302 throughout the embryo, which then becomes increasingly localized to anterior structures before being largely silenced.

Neural Tube Closure Defects and Embryonic Lethality in *mir-302* Knockouts

The *mir-302* cluster produces four highly similar miRNAs (miR-302a-d) that share the seed sequence *aagugcu*, as well as an unrelated miRNA, miR-367 (Figure 2A). To study the role of miR-302 in embryonic development, we genetically deleted *mir-302a-d* by replacing the hairpin structures with the coding region of enhanced GFP (eGFP) (Figure 2B). Resulting heterozygous mice showed no discernible phenotype. However, heterozygous intercrosses failed to produce any knockout mice (n = 621). Genotyping of embryos showed a large decrease in the number of knockouts observed between E15.5 and E17.5 and no recoverable knockouts at E18.5 (Figure 2C).

At E7.5, knockout embryos appeared normal and could be identified by higher levels of GFP expression compared with their heterozygous littermates (Figure 2D). They had normal size and normal morphological features (Figures 2D, S2A, and S2B). Genotyping and qRT-PCR confirmed the loss of miR-302 but not miR-367 expression in knockout embryos. The *mir-302* cluster is antisense to an intron of another gene *Larp7*, which encodes part of the 7SK small nuclear ribonucleoprotein particle (He et al., 2008). *mir-302a-d* knockout embryos showed a small, statistically insignificant reduction in the expression of *Larp7*; thus, deletion of *mir-302* appeared to have little to no effect on this gene (Figure S2C). Notably, mice heterozygous for *Larp7* have no discernible phenotype (Okamura et al., 2012).

Although E7.5 knockout embryos appeared normal, E9.5 embryos were grossly abnormal, with large open anterior neural tubes encompassing the mid and hindbrain, with variable extension into the forebrain region (Figure 2E). This 100% penetrant phenotype was a striking contrast to the phenotypes of wild-type and heterozygous littermates, which consistently had closed neural tubes at this time point. In *mir-302* knockouts, the neural tube remained open throughout the remainder of development, resulting in severely abnormal brain development and thickened exencephalic hindbrains at E13.5 (Figure S2D).

Transverse sections of the mid and hindbrain showed a failure of dorsolateral hinge formation and neural tube closure, eventually resulting in a collapse of the neural fold by E10.5 (Figure 2F). Abnormal eye development was also evident in the knockout embryos (Figure 2E). Together, these results show an essential role for miR-302a-d in early neural development.

Thickening of the Neuroepithelium in *mir-302* Knockouts

To determine the cellular basis of the neural tube defect, we dissected and carefully evaluated neural development in the knockouts. Neurulation is the process by which the flat neural plate folds into a neural tube along the anterior-posterior axis of vertebrates. It is influenced by multiple cellular processes, including but not limited to proliferation, apoptosis, differentiation, apical constriction, and patterning (Copp et al., 2003; Greene et al., 2009; Greene and Copp, 2014). Murine cranial neurulation occurs from ~E8.25 to E9.25. Early in neurulation at E8.5, there was no significant difference in the total number of cells in the neuroepithelium between wild-type and knockout embryos (Figures 3A and S3A). By E9.5, however, there was an approximately 25% increase in the total number of cells in matching transverse sections of the hindbrain, along with an equivalent increase in the thickness of the neural epithelium (Figure 3A). Similar to the increases in cellular number in the hind-brain, increased thickness of the midbrain and forebrain were observed (Figure S3B).

To understand the mechanism of neuroepithelial expansion between E8.5 and E9.5, we analyzed markers of cellular proliferation and apoptosis. Staining for phospho-histone H3 (PH3) revealed a significant increase in the number of cells in M phase in knockout neuroepithelium at E8.5 but not at E9.5 (Figures 3B and S3C). To analyze the S phase, we performed bromodeoxyuridine (BrdU)-labeling experiments and found a significant increase in BrdU-positive cells at E8.5 but not E9.5 (Figure 3C). Furthermore, analysis of apoptosis by both cleaved Caspase3 immunohistochemistry and TUNEL staining showed a 5- to 10-fold decrease in apoptosis at E9.5 but little to no change at E8.5 (Figures 3D and S3D–S3F). Consistent with the apoptosis data, LysoTracker staining for dead cells in whole-mount embryos showed a striking reduction in cell death in the hind and midbrain region of E9.5 embryos (Figure 3E). Together, these data show an expansion in neuroepithelium associated with early increases in proliferation and late decreases in apoptosis during neurulation of the knockout embryos.

Precocious Neuronal Differentiation in *mir-302* Knockouts

Next, we asked whether there were defects in neuronal differentiation and patterning in *mir-302*-knockout embryos. Tuj1 (acetylated β-III tubulin) marks early post-mitotic neurons, which are first seen in the cranial region in very small numbers following the completion of neurulation at about E9.5. Staining for Tuj1 in the hindbrain at E8.5 showed no staining in either wild-type or knockout neural tubes. However, small numbers of Tuj1+ cells were seen in knockout hindbrains as early as E9.0 but not in wild-type (Figure S4-1A). By E9.5, there was a striking increase in the number of Tuj1+ cells in both the midbrain and hindbrain of the knockout embryos compared with wild-type (Figures 4A, S4-1B, and S4-1C). This finding was confirmed with the other neuronal markers, including *Elavl2* and *Neurofilament*

(*NF*) (Figures S4-1D and S4-1E). Simultaneous immunostaining for Ki67, a marker of cycling progenitors, revealed a small but significant increase in the number of total Ki67+ cells as well as Tuj1+/Ki67+ cells in knockout embryos compared with wild-type, which is consistent with the simultaneous expansion of progenitors and precocious differentiation (Figure 4B).

To further evaluate neurogenesis, we stained for *Btg2 (Tis21)*. *Btg2* is expressed in and required for neurogenic progenitor divisions starting around E9.5 (Iacopetti et al., 1999; Farioli-Vecchioli et al., 2009). *mir-302*-knockout embryos showed increased Btg2 expression at E9.5 and E10.5 (Figures 4C and S4-1F). At E9.5, increased expression was seen in the mid and hindbrain region. By E10.5, the difference was dramatically more pronounced and could be found to extend into the forebrain region. In addition to *Btg2*, other markers of neuroepithelial progenitors, such as *Hes1* and *Hes5*, were analyzed (Ishibashi et al., 1995; Hatakeyama et al., 2004). *Hes5* showed increased staining in the midbrain and hindbrain at both E8.5 and E9.5 (Figures 4D and S4-1G). Similarly, *Hes1* also showed ectopic expression in the hindbrain neuroepithelium at E9.5 that extended into the midbrain and forebrain (Figure S4-1H).

To more directly measure neurogenic divisions, we performed analysis of daughter pairs arising from individual dividing cells derived from dissociated anterior neural tubes. Individual dividing cells had three possible outcomes: symmetric division into two Tuj1− progenitors (P/P), symmetric division into two Tuj1+ neurons (N/N), or asymmetric division into one Tuj1+ progenitor and one Tuj1+ neuron (P/N) (Figure 4E). Quantification of these divisions showed a preponderance of the P/P divisions in both wild-type and knockout embryos (~90%). However, there was a small yet highly significant increase in the number of N/N divisions in knockout embryos (Figure 4E). There was also a trend toward increased P/N divisions ($p = 0.35$). Together, these findings show that the loss of *mir-302* leads to premature neurogenesis along with expansion of the neural progenitor pool during neurulation of the cranial neural tube.

In contrast to the changes in proliferation, apoptosis, and differentiation, there did not appear to be any changes in embryonic axis specification associated with *mir-302* loss. Knockout mice showed normal anterior-posterior patterning, as indicated by *FoxG1* (forebrain), *En-2*, *Gbx2* (midbrain), and *Krox20* (hind-brain) expression (Figure S4-2A and S4-2B). Additionally, there were no obvious differences in dorsal or ventral patterning of the spinal cord at E9.5, as measured by *Msx1/2*, *Pax3*, *Pax6*, and *Nkx2.2* immunostaining (Figure S4-2C).

Multiple Target mRNAs Are Upregulated in *mir-302* Knockouts

To understand the molecular basis underlying the *mir-302* neurulation defect, we next searched for targets of miR-302 in the context of the anterior neural plate/neural tube. miRNAs regulate both translation and mRNA stability. Therefore, mRNA targets should be increased in the *mir-302*-knockout background. Although the gross phenotype of the knockout embryos is evident only beginning at E9.5, the molecular defects underlying this outcome likely precede this event. Indeed, by E9.5, miR-302 levels were already down approximately 6-fold from their peak at E7.5 (Figure 1B). Therefore, we performed mRNA

profiling on wild-type and knockout littermates at multiple time points encompassing E7.5 to E9.5 (Figure 5A). All time points were defined by matching somite counts. Surprisingly, very few targets were significantly misregulated at E7.5. This may be due to the closely related miRNA family members expressed from the *mir-290* cluster, whose expression overlaps with early *mir-302* expression (Figure 5B) (Parchem et al., 2014). In addition, for technical reasons, the entire embryo was used at E7.5 for profiling expression; therefore, microarray results reflect a heterogeneous mix of tissues with highly distinct expression patterns. Beginning at E8.0, however, it was possible to specifically isolate the anterior neural plate for profiling.

Among the genes that were upregulated in knockout embryos, there was a strong enrichment for the complementary sequence to the miR-302 seed in their 3′UTR and to a lesser extent open reading frames (ORFs), even at E7.5, when few genes had altered mRNA expression levels (Figure 5A). By E8.0, hundreds (426) of genes were misregulated in the knockout anterior neural plate, and this number continued to increase with further development (E8.5 and E9.5). By E9.5, there was no longer an enrichment of the miR-302 seed motif in the upregulated gene set, consistent with most of the molecular defect being the secondary consequence of earlier expression changes. Gene Ontology analysis of the E9.5 changes showed a strong enrichment for categories associated with neurogenesis, thus validating our phenotypic analyses of premature neuronal differentiation but not providing much insight into the critical miR-302 targets (Figure 5C). Therefore, we focused on earlier time points. The expression of ten representative genes that were upregulated at one of these time points and had seed sequence matches to miR-302 were validated by qRT-PCR (Figure 5D). Surprisingly few of the uncovered miR-302 targets were misexpressed at multiple time points. Indeed, among all misregulated genes with seed matches, only two were consistently upregulated from E8.0 through E9.5: *Fgf15* and *Ednrb* (Figure 5E). *Fgf15* was intriguing, as previous work suggested that this gene is important for neurogenesis (Borello et al., 2008; Fischer et al., 2011; Miyake et al., 2005). Interestingly, qRT-PCR showed that the degree of *Fgf15* overexpression in *mir-302* knockouts increased with each developmental stage tested unlike the other nine targets analyzed. Therefore, *Fgf15* was a strong candidate for further characterization.

Fgf15 Is a Direct Target of miR-302 and Can Induce Premature Neurogenesis

To validate *Fgf15* as a direct target of miR-302 in the anterior neural tube, we performed in situ hybridization, western blotting, and luciferase assays (Figures 6A, 6B, S6A, and S6B). In situ hybridization showed increased levels of Fgf15, which correlated well with our qRT-PCR results (Figures S6A and S6B). Western blots showed that the protein was also upregulated (Figure 6A). Luciferase activity was suppressed by miR-302 in constructs carrying the 3′UTR of *Fgf15* but not in constructs with a seed sequence mutation within the 3′UTR (Figure 6B). Therefore, *Fgf15* is a direct target of miR-302 in the context of the developing anterior neural tube.

To test whether overexpression of *Fgf15* is sufficient to drive precocious neural differentiation, we used viral overexpression to ectopically express *Fgf15* in chick embryos during neurulation. Anterior neural tissue prior to neurulation was infected at HH stage 6–7,

allowed to develop for 72 hr, and then analyzed for neurogenesis. Whole-mount staining and phenotypic analysis revealed robust infection and gross morphological defects within anterior neural structures associated with *Fgf15* overexpression (Figure 6C). To quantify the effect of *Fgf15* on neurogenesis, we used pair analysis to compare neurogenic potential of infected and non-infected cells within the same embryo (Figure 6D). *Fgf15*-overexpressing cells were more likely to give rise to neurons than uninfected cells (Figure 6E). In contrast, overexpression of GFP did not result in an increase in neurogenesis. Together, these findings show that *Fgf15* is a direct target of miR-302 and its mis-expression recapitulates aspects of the precocious differentiation phenotype seen with *mir-302* loss.

miR-302/miR-290 Double Knockouts Arrest Prior to Neurulation

The timing of the *mir-302* phenotype was relatively late during the window of expression for this cluster. Earlier roles of *mir-302* could be masked by the co-expression of the *mir-290* cluster, which shares multiple miRNAs with the same seed sequence as miR-302a-d. Expression of *mir-302* and *mir-290* overlap from ~E5.5–E7.5 (Figure 7A). To test potential redundant roles for these two clusters, we produced compound mutants by intercrossing *mir-302*/*mir-290* heterozygous mice. The loss of any three or four of the four alleles led to a decrease in the number of recoverable mutant embryos at E9.5 (Figures 7B and 7C). Recovered embryos could not be appropriately staged, as they were highly abnormal, although double knockouts had clearly arrested prior to neurulation. Thus, the combination of *mir-302* and *mir-290* mutant alleles results in an early synthetic lethal phenotype. These results demonstrate a role for *mir-302* prior to neurogenesis that is redundant with *mir-290*. Future studies will be required to understand the cellular basis for this phenotype.

DISCUSSION

Neurulation is a defining feature of vertebrate development and is essential for proper CNS development and embryonic viability (Zhong et al., 2000; Hatakeyama et al., 2004; Oka et al., 1995; Copp and Greene, 2010; Copp et al., 2003; Greene and Copp, 2014). A failure in neural tube closure is one of the most common birth defects, due in part to the complex choreography required to bend, fold, and fuse the embryonic neural tissue while accurately timing the proliferation, apoptosis, and differentiation of neural precursors (Copp et al., 2003; Copp and Greene, 2010; Greene and Copp, 2014). Here, miR-302 is identified as a critical and pleiotropic regulator of neuroepithelial differentiation during neurulation. Specifically, miR-302 represses premature expansion of progenitors and production of post-mitotic neurons (Figure 7D). Knockout embryos fail to close the neural tube and eventually die, representing a fully penetrant embryonic lethal miRNA knockout phenotype.

The uncovered cellular phenotypes are consistent with an accelerated neural differentiation program, suggesting that miR-302 functions as a developmental timer. Let-7, one of the earliest miRNAs discovered, has also been proposed to act as a developmental timer, regulating the timing of differentiation of several lineages in *C. elegans* (Reinhart et al., 2000). Moreover, let-7 has recently been shown to regulate the timing of the neurogenic to gliogenic transition during mouse neural development (Patterson et al., 2014; Nishino et al.,

2013). miR-302 functions opposite to let-7, as its loss leads to an acceleration, rather than a delay in differentiation. Interestingly, miR-302 and let-7 have been shown to have antagonistic roles through the opposing effects on multiple downstream pathways in vitro (Melton et al., 2010). Similar antagonism is likely to occur in vivo to regulate the timing of cell fate decisions.

Fgf15 is a direct target of miR-302 in the context of neurulation. Previous analysis of *Fgf15* knockout mice reported a delay in neurogenesis and increased proliferation in the cortex of E12.5 and E14.5 mice, uncovering a requirement for this signaling factor in cell-cycle exit and differentiation into neurons (Borello et al., 2008). Here, we find that *Fgf15* overexpression, as seen with miR-302 loss, results in premature neurogenesis, showing that it is not only necessary but also sufficient for the induction of differentiation in the appropriate cell context. The previous association of *Fgf15* loss with increased proliferation, though, seemingly contradicts our results showing increased proliferation secondary to loss of miR-302 and increased *Fgf15* expression. Interestingly, morpholino-induced knockdown of the zebrafish homolog *Fgf19* results in reduced proliferation and increased apoptosis in the dorsal regions of the developing dorsal forebrain, midbrain, and cerebellum (Miyake et al., 2005). These differences in *Fgf15* function likely reflect differences in cellular context both in terms of developmental time and place. Our *mir-302*-knockout phenotype is consistent with aspects of the previously described *Fgf15* functions. However, changes in *Fgf15* alone cannot explain the multiple cellular phenotypes uncovered.

Many targets of miR-302 were uncovered in this study. Furthermore, many other miR-302 targets have been previously described, particularly in the setting of pluripotency (Lipchina et al., 2011). Surprisingly, our analysis shows little overlap with this previous work but rather identifies hundreds of distinct targets showing the importance of cellular context on the repertoire of targets influenced by any particular miRNA. Indeed, even within the context of neuroepithelial differentiation, the targets were rapidly changing over time. Interestingly, the phenotypes uncovered here for miR-302 are the opposite of those previously described for miR-302 and its related ESCC family members in other contexts. In particular in ESCs, the ESCC family promotes cell cycle and inhibits apoptosis (Zheng et al., 2011; Wang et al., 2008, 2013; Pernaute et al., 2014; Qi et al., 2009). Again, this contradiction emphasizes the importance of cellular context on miRNA function. Furthermore, it highlights the importance of studying miRNAs in vivo as well as in vitro. Previous in vitro work on the role of miR-302 on human ESC differentiation suggested an important role in mesendoderm specification (Rosa et al., 2009). However, the knockout embryos show no obvious defect in the formation of early mesendoderm, although more subtle phenotypes may be uncovered with further detailed characterization of mesendoderm derived structures. Indeed, Tian et al. (2015) recently published a conditional deletion of the entire *mir-302* cluster, including *miR-367*, specifically in the developing heart. Resulting mice were viable but showed ventricular wall thinning and septum hypoplasia associated with a decrease in Ki67+ cells.

A small number of studies have suggested important roles for related miRNAs in non-mammalian species. For example, in teleost (fish), miR-430 (miR-302 ortholog) has been implicated in several developmental functions. Specifically, miR-430 was shown to degrade

maternal transcripts at the maternal-zygotic transition in zebrafish (Giraldez et al., 2006). Additionally, zebra-fish embryos lacking all miRNAs have defects in brain morphogenesis that are rescued by reintroduction of miR-430 (Giraldez et al., 2005). Therefore, our results suggest conserved function for this family of miRNAs during vertebrate neurulation, although a more definitive comparison awaits an understanding of the cellular basis of the zebrafish defect. The clearing of maternal transcripts is unlikely to be a conserved function for miR-302, as it is not expressed until 3 days after the maternal-to-zygotic transition. However, such a function may be accomplished by miR-290, which, similar to miR-430, is upregulated shortly after fertilization at the time of zygotic gene activation (Tang et al., 2007). In amphibians, the miR-302 ortholog miR-427 has been described to play a role in gastrulation (Rosa et al., 2009). This earlier role may be masked in mammals by the co-expression of the *mir-290* and *mir-302* clusters, which could be acting redundantly. Our analysis of compound *mir-290*/*mir-302* mutants is consistent with an earlier function for miR-302 during gastrulation. The observation that removal of miR-302 and miR-290 leads to more severe defects than either alone strongly supports this idea. Because expression of miR-302 family miR-NAs is conserved across vertebrate development during gastrulation, it likely plays an evolutionarily conserved role during germ layer formation, which in mice is redundant with miR-290. It is interesting to speculate that the evolution of the *mir-290* cluster allowed unique temporal control of expression in embryonic versus extra-embryonic tissues and could thus have played a role in placental evolution while maintaining robust regulation of gastrulation.

Analyses of miRNA knockouts in mice have uncovered largely variable and incompletely penetrant phenotypes, with many knockouts showing no obvious phenotype at all (Park et al., 2010; Vidigal and Ventura, 2015). A similar absence of phenotypes has been described for most miRNA knockouts in *C. elegans* (Alvarez-Saavedra and Horvitz, 2010; Miska et al., 2007). Compound mutants of homologous clusters can lead to more severe phenotypes consistent with redundancy (Park et al., 2010; Ventura et al., 2008; Heidersbach et al., 2013). However, none of these resulted in fully penetrant embryonic lethal phenotypes. Thus, miRNAs are generally considered to be fine-tuners of gene expression that buffer biological systems from environmental perturbation. Our findings contradict this notion, as they show that a single cluster of related miRNAs plays a central role in neural development. Therefore, the coordinated regulation of mRNA degradation and translation of specific mRNAs by miRNAs is more than a buffer against environmental perturbation; it can also be part of an evolutionarily conserved developmental mechanism.

EXPERIMENTAL PROCEDURES

Genotyping

Mouse genomic DNA was isolated from toes of postnatal mice or tails of embryos. Tissue was digested in lysis buffer (50 mM Tris-HCl [pH 8.0], 10 mM EDTA, 100 mM NaCl, 0.1% SDS, and 5mg/ml proteinase K) overnight at 55ºC. DNA was isolated by the addition of equal volume isopropanol, vortexing, and then a 5 min centrifugation. Isopropanol was removed, and samples were allowed to air dry. After the addition of H_2O, samples were again vortexed and heated at 85ºC for 5 min and spun down. PCR was performed using

primer pairs to distinguish the miR-302 wild-type (L: ctctttgggaggcggtcacg; R: gagac agaaagcattcccatg) and mutant (L: ctctttgggaggcggtcacg; R: cttgccgtaggtggcatcgc). PCR conditions were 35 cycles at 94ºC for 30 s, 52ºC for 30 s, and 72ºC for 45 s. Band sizes were as follows: wild-type is 154 bp, while the mutant band is 216 bp. miR-302 GFP primers are as follows: wild-type (L: caggacctactttccccagagctg; R: gaacccacccacaaggcaactag) and mutant (L: caggacctactttccccagagctg; and R: gaagatggtgcgctcctggacgtagc). PCR conditions were as previously described, except with an adjustment of the annealing temperature to step down 64ºC, 62ºC, and 60ºC. Band sizes for genotyping were as follows: wild-type band at 274 bp and GFP band at 547 bp.

Histology and Immunohistochemistry

Embryos were dissected in PBS, fixed in 4% paraformaldehyde in PBS at 4ºC overnight, cryoprotected in 30% sucrose at 4ºC overnight, in 1:1 30% sucrose: OCT at 4ºC overnight, embedded in OCT and stored at −80ºC until use. Cryomicrotome sectioning was done at 10–12 μm. Sections were stored at −80ºC prior to immunohistochemistry staining. For BrdU staining, 50 mg BrdU/kg weight was injected 2 hr prior to embryo collection. BrdU-labeled cryosections were then steamed in 10 mM citrate buffer (pH 6) for 20 min at 99ºC for antigen retrieval. Sections were blocked with 5% goat serum/PBS 0.1% Tween 20, incubated in primary antibody in blocking solution at 4ºC overnight (BrdU 1:1,000 [AbCam ab6326]; GFP 1:100 [Living Colors Clontech 632381]; PH3 1:500 [Cell Signaling 9701S]; TUJ1 1:1,000 [Covance MMS-435P-250]; Ki67 1:500 [Thermo Scientific #RM-9106-S1]; Isl1-2 1:200 [Developmental Studies Hybridoma Bank (DSHB) 40.3A4-S]; NF 1:500 [AbCam ab65845]; Caspase3 1:400 [Cell Signaling 9664]; Pax3 1:200 [DSHB pax3]; Pax6 1:200 [DSHB pax6]; Nkx2.2 1:200 [DSHB 74.5A5-S]; Msx1/2 1:200 [DSHB 4G1]; and Elavl2 1:250 [Proteintech Group 14008-1-AP]). Secondary antibodies (AlexaFluor) in blocking buffer were applied for 2 hr at room temperature. For quantification of apoptosis, fluorescent TUNEL assays (TREVIGEN TACS.XLT 4828-30-DK) were performed on cryosections per the manufacturer's instructions for labeling. Rat anti-BrdU antibody (AbCam) was then used for subsequent immunofluorescence staining. For whole-mount LysoTracker evaluation of cell death, embryos were dissected in PBS, incubated in LysoTracker Red 1:5,000 (Life Technology L7528) for 45 min at 37ºC. Samples were then washed twice in PBS and imaged.

Western Blots

Embryos were dissected as previously described, and E9.5 dorsal telencephalon explants were isolated. Samples were lysed in lysis buffer (25 mM Tris at [pH 7.9], 150 mM NaCl, 0.1 mM EDTA, 0.1% Triton X-100, 10% glycerol, and 1 mM DTT) as well as 1X Proteinase Inhibitor Cocktail (Roche) and 1x PhosSTOP Phosphatase Inhibitor Cocktail (Roche). Samples were then treated to at least cycles of snap freeze and thaw at −80ºC and stored at −80ºC until use. Protein was quantified with a Bio-Rad protein assay. Five to seven micrograms of protein was resolved by SDS-PAGE (Bio-Rad 4%–15% Mini-PROTEAN TGX Gel). Protein was then transferred to Immobilon-FL (Millipore), further processed by immunodetection, and blots scanned on a Li-Cor Odyssey Scanner. Antibody dilutions were Fgf15 1:200 (Santa Cruz; sc-16816) and GAPDH 1:1,000 (Santa Cruz; sc-365062).

Secondary infrared-dye antibodies from Li-Cor used were diluted 1:15,000. Odyssey Software was used to quantify images.

qRT-PCR

E7.5, E8.5, and E9.5 wild-type and mutant dorsal telencephalon explants were isolated as described, lysed in 700 μl of Trizol, and stored at −20ºC. RNA was isolated and purified (miRNeasy micro kit) according to the manufacturer's instructions. cDNA was generated for miRNA and mRNA by reverse transcription with oligo-dT primers (Invitrogen Superscript Kit). Gene-specific primers (500 nM) and Power SYBR Green PCR Master Mix (Life Technologies) were used. PCR quality controls, experimental runs, and statistical methods were performed as described (Shi and Chiang, 2005). Primer sequences can be found in the Supplemental Experimental Procedures.

Gene Targeting

Mir-302 heterozygous knockout ESCs were generated by inserting the coding region for eGFP in place of the miR-302a-d hairpin sequences. Genomic homology arms encompassing *mir-302* clusters were sub-cloned from BACs into pL253 targeting vectors by recombineering. Fluorescent proteins adjacent to SV40pA were cloned into the pL452 recombineering vector next to the floxed neomycin cassette. The fluorescent protein/SV40 polyA and floxed neomycin cassette were then inserted in place of the miR-302a-d hairpins in the pL253-targeting constructs using recombineering. pL253-targeting constructs were linearized and electroporated (20 μg) into V6.5 ESCs followed by selection with Geneticin (G418, 200 μg/ml) for 7 days. Sub-clones were screened for proper targeting using long-range PCR. Primers specific to the transgene (i.e., fluorescent protein/neomycin cassette) and genomic regions outside the homology arms of the targeting construct were used to screen for properly targeted colonies. The resulting targeted clones were transfected with a Cre recombinase-expressing plasmid to remove the neomycin cassette. PCR was used to screen sub-clones for loss of neomycin.

Daughter Pair Analysis

Daughter pair analysis was done as previously described (Qian et al., 1998). Briefly, cranial neural tissue was isolated from E9.5 embryos, dissociated into single cells, and plated in poly-L-lysine coated wells. The single cells were incubated at 37ºC, 5% CO_2, and 100% humidity. Daughter pair cells were identified after 24 hr incubation by fixing with 4% formaldehyde and staining for Tuj1 and DAPI.

Luciferase Assay

All experiments were performed using the Dual-Luciferase Reporter Assay System (Promega) on a dual-injecting SpectraMax L (Molecular Devices) luminometer according to the manufacturer's protocol. Ratios of Renilla luciferase readings to firefly luciferase readings were averaged for each experiment. Replicates performed on separate days were mean-centered with the readings from the individual days. For target verification reporter assay, 3′UTRs of indicated genes were amplified from the mouse genomic DNA cells using the Zero Blunt TOPO (Invitrogen) vector and sub-cloned into psiCHECK-2 vector

(Promega) using the Cold Fusion Cloning Kit (System Biosciences). 3′UTR seed sequences were mutated using the Quickchange Lightning kit (Agilent). For transfection, 8,000 miRNA-deficient Dgcr8−/− mouse ESCs were plated in ESC media onto a 96-well plate pretreated with 0.2% gelatin. The subsequent day, the cells were transfected with miRIDIAN miRNA mimics (Dharmacon) using Dharmafect1 (Dharmacon) at the manufacturer's recommended concentration of 100 nM. Simultaneously, 200 ng of the psiCHECK-2 construct was transfected into the ESCs using Fugene6 (Roche) transfection reagent according to the manufacturer's protocol. Transfection of each construct was performed in triplicate in each assay. The cells were lysed 24 hr after transfection, and the luciferase assay was performed.

RNA Microarray Analysis

For mRNA analysis of embryonic tissue during development, total RNA was isolated from dissected anterior neural tissue from E8.0–E9.5 and whole embryos isolated from extra-embryonic tissues at E7.5 using miR-Neasy micro columns (Qiagen) according to the manufacturer's protocol. Triplicate biological samples were analyzed using Illumina MouseRef-8 v2.0 Expression BeadChips run by the UCLA Neuroscience Genomics Core. Microarray data were preprocessed, and quality control was performed using Illumina BeadArray software and the SampleNetwork R function (Oldham et al., 2012). This analysis revealed one sample outlier ($Z.K < -3$), which was removed prior to quantile normalization. Seed sequence enrichment was performed as previously described (Melton et al., 2010).

In Situ Hybridization

Digoxigenin-labeled probes were prepared and purified using RNeasy columns (Qiagen). Whole-mount in situ hybridization was performed as follows: embryos were rehydrated in PT (1× PBS [pH 7.4] and 0.01% Triton X-100) and fixed for 30 min in a 9:1 mixture of PT to 37% formaldehyde. The embryos were then washed in PT and incubated in hybridization buffer (5× SSC [pH 4.5], 1% SDS, 50% Formamide) at 65ºC for 1–2 hr. Probe was added to the embryos at a final concentration of 0.25–5 ng/μl in hybridization buffer and incubated for 12–18 hr at 65ºC. After probe removal, embryos were washed several times in hybridization buffer at 65ºC over 2–4 hr. Embryos were then washed several times in PT at room temperature for 1 hr. This was followed by incubating overnight with antibody at 4ºC (Boehringer-Mannheim anti-digoxigenin/fluorescein-alkaline phosphatase [AP]) diluted (1:3,000) in PT overnight at 4ºC. The embryos were then washed several times in PT for 1 hr before washing in AP buffer (5 mM $MgCl_2$, 100 mM NaCl, 100 mM Tris [pH 9.5], 0.1% Tween-20) for 30 min at room temperature. The embryos were reacted in BM Purple (Boehringer-Mannheim) for 1–24 hr in the dark at room temperature. After the reaction, embryos were washed with PT, stained with DAPI, and imaged.

Retroviral Overexpression of Target Genes in Chick Embryos

Gene overexpression was targeted to the chick neuroepithelium via infection with the RCASBP(B) viral construct (Hughes, 2004). Fgf15 was cloned into the RCAS (B) construct using ColdFusion following the manufacturer's protocol (SBI). RCAS-BP virus was produced by infecting DF-1 cells with the SuperFect Transfection Reagent (Qiagen), and then harvesting the viral supernatant as previously described (Morgan and Fekete, 1996).

Virus was injected with a trace amount of Fast Green tracer dye into HH6 neural folds of virus-free SPAFAS chick embryos (Charles River Labs) using glass micropipettes and a Picospritzer fluid injector. Control embryos were injected with RCASBP(B)-GFP.

Animal Use

All animal experiments in this article were approved by the Institutional Animal Care and Use Committee of the University of California, San Francisco.

Supplementary Material

Refer to Web version on PubMed Central for supplementary material.

Acknowledgments

R.J.P. was supported by grants T32 HD007263 and F32 HD070572 from the NIH. R.B. was supported by grants R01 GM101180 and U54 HD055764 from the NIH and by grant RN2-00906-1 from the California Institute of Regenerative Medicine. J.L.R.R. was supported by grant R01 NS34661 from the NIH. R.A.S. was supported by grant R01 DE016402 from the NIH.

References

Abbott AL, Alvarez-Saavedra E, Miska EA, Lau NC, Bartel DP, Horvitz HR, Ambros V. The let-7 MicroRNA family members mir-48, mir-84, and mir-241 function together to regulate developmental timing in Caenorhabditis elegans. Dev Cell. 2005; 9:403–414. [PubMed: 16139228]

Alvarez-Saavedra E, Horvitz HR. Many families of C. elegans microRNAs are not essential for development or viability. Curr Biol. 2010; 20:367–373. [PubMed: 20096582]

Bartel DP. MicroRNAs: target recognition and regulatory functions. Cell. 2009; 136:215–233. [PubMed: 19167326]

Bernstein E, Kim SY, Carmell MA, Murchison EP, Alcorn H, Li MZ, Mills AA, Elledge SJ, Anderson KV, Hannon GJ. Dicer is essential for mouse development. Nat Genet. 2003; 35:215–217. [PubMed: 14528307]

Borello U, Cobos I, Long JE, McWhirter JR, Murre C, Rubenstein JL. FGF15 promotes neurogenesis and opposes FGF8 function during neocortical development. Neural Dev. 2008; 3:17. [PubMed: 18625063]

Card DA, Hebbar PB, Li L, Trotter KW, Komatsu Y, Mishina Y, Archer TK. Oct4/Sox2-regulated miR-302 targets cyclin D1 in human embryonic stem cells. Mol Cell Biol. 2008; 28:6426–6438. [PubMed: 18710938]

Copp AJ, Greene ND. Genetics and development of neural tube defects. J Pathol. 2010; 220:217–230. [PubMed: 19918803]

Copp AJ, Greene ND, Murdoch JN. The genetic basis of mammalian neurulation. Nat Rev Genet. 2003; 4:784–793. [PubMed: 13679871]

Ebert MS, Sharp PA. Roles for microRNAs in conferring robustness to biological processes. Cell. 2012; 149:515–524. [PubMed: 22541426]

Farioli-Vecchioli S, Saraulli D, Costanzi M, Leonardi L, Cinà I, Micheli L, Nutini M, Longone P, Oh SP, Cestari V, Tirone F. Impaired terminal differentiation of hippocampal granule neurons and defective contextual memory in PC3/Tis21 knockout mice. PLoS ONE. 2009; 4:e8339. [PubMed: 20020054]

Fischer T, Faus-Kessler T, Welzl G, Simeone A, Wurst W, Prakash N. Fgf15-mediated control of neurogenic and proneural gene expression regulates dorsal midbrain neurogenesis. Dev Biol. 2011; 350:496–510. [PubMed: 21172336]

Giraldez AJ, Cinalli RM, Glasner ME, Enright AJ, Thomson JM, Baskerville S, Hammond SM, Bartel DP, Schier AF. MicroRNAs regulate brain morphogenesis in zebrafish. Science. 2005; 308:833–838. [PubMed: 15774722]

Giraldez AJ, Mishima Y, Rihel J, Grocock RJ, Van Dongen S, Inoue K, Enright AJ, Schier AF. Zebrafish MiR-430 promotes deadenylation and clearance of maternal mRNAs. Science. 2006; 312:75–79. [PubMed: 16484454]

Greene ND, Copp AJ. Neural tube defects. Annu Rev Neurosci. 2014; 37:221–242. [PubMed: 25032496]

Greene ND, Stanier P, Copp AJ. Genetics of human neural tube defects. Hum Mol Genet. 2009; 18(R2):R113–R129. [PubMed: 19808787]

Greve TS, Judson RL, Blelloch R. microRNA control of mouse and human pluripotent stem cell behavior. Annu Rev Cell Dev Biol. 2013; 29:213–239. [PubMed: 23875649]

Hatakeyama J, Bessho Y, Katoh K, Ookawara S, Fujioka M, Guillemot F, Kageyama R. Hes genes regulate size, shape and histogenesis of the nervous system by control of the timing of neural stem cell differentiation. Development. 2004; 131:5539–5550. [PubMed: 15496443]

He N, Jahchan NS, Hong E, Li Q, Bayfield MA, Maraia RJ, Luo K, Zhou Q. A La-related protein modulates 7SK snRNP integrity to suppress P-TEFb-dependent transcriptional elongation and tumorigenesis. Mol Cell. 2008; 29:588–599. [PubMed: 18249148]

Heidersbach A, Saxby C, Carver-Moore K, Huang Y, Ang YS, de Jong PJ, Ivey KN, Srivastava D. microRNA-1 regulates sarcomere formation and suppresses smooth muscle gene expression in the mammalian heart. eLife. 2013; 2:e01323. [PubMed: 24252873]

Houbaviy HB, Murray MF, Sharp PA. Embryonic stem cell-specific microRNAs. Dev Cell. 2003; 5:351–358. [PubMed: 12919684]

Houbaviy HB, Dennis L, Jaenisch R, Sharp PA. Characterization of a highly variable eutherian microRNA gene. RNA. 2005; 11:1245–1257. [PubMed: 15987809]

Hughes SH. The RCAS vector system. Folia Biol (Praha). 2004; 50:107–119. [PubMed: 15373344]

Iacopetti P, Michelini M, Stuckmann I, Oback B, Aaku-Saraste E, Huttner WB. Expression of the antiproliferative gene TIS21 at the onset of neurogenesis identifies single neuroepithelial cells that switch from proliferative to neuron-generating division. Proc Natl Acad Sci U S A. 1999; 96:4639–4644. [PubMed: 10200315]

Ishibashi M, Ang SL, Shiota K, Nakanishi S, Kageyama R, Guillemot F. Targeted disruption of mammalian hairy and Enhancer of split homolog-1 (HES-1) leads to up-regulation of neural helix-loop-helix factors, premature neurogenesis, and severe neural tube defects. Genes Dev. 1995; 9:3136–3148. [PubMed: 8543157]

Jouneau A, Ciaudo C, Sismeiro O, Brochard V, Jouneau L, Vandormael-Pournin S, Coppée JY, Zhou Q, Heard E, Antoniewski C, Cohen-Tannoudji M. Naive and primed murine pluripotent stem cells have distinct miRNA expression profiles. RNA. 2012; 18:253–264. [PubMed: 22201644]

Lipchina I, Elkabetz Y, Hafner M, Sheridan R, Mihailovic A, Tuschl T, Sander C, Studer L, Betel D. Genome-wide identification of microRNA targets in human ES cells reveals a role for miR-302 in modulating BMP response. Genes Dev. 2011; 25:2173–2186. [PubMed: 22012620]

Medeiros LA, Dennis LM, Gill ME, Houbaviy H, Markoulaki S, Fu D, White AC, Kirak O, Sharp PA, Page DC, Jaenisch R. Mir-290-295 deficiency in mice results in partially penetrant embryonic lethality and germ cell defects. Proc Natl Acad Sci U S A. 2011; 108:14163–14168. [PubMed: 21844366]

Melton C, Judson RL, Blelloch R. Opposing microRNA families regulate self-renewal in mouse embryonic stem cells. Nature. 2010; 463:621–626. [PubMed: 20054295]

Miska EA, Alvarez-Saavedra E, Abbott AL, Lau NC, Hellman AB, McGonagle SM, Bartel DP, Ambros VR, Horvitz HR. Most Caenorhabditis elegans microRNAs are individually not essential for development or viability. PLoS Genet. 2007; 3:e215. [PubMed: 18085825]

Miyake A, Nakayama Y, Konishi M, Itoh N. Fgf19 regulated by Hh signaling is required for zebrafish forebrain development. Dev Biol. 2005; 288:259–275. [PubMed: 16256099]

Morgan BA, Fekete DM. Manipulating gene expression with replication-competent retroviruses. Methods Cell Biol. 1996; 51:185–218. [PubMed: 8722477]

Nishino J, Kim S, Zhu Y, Zhu H, Morrison SJ. A network of heterochronic genes including Imp1 regulates temporal changes in stem cell properties. eLife. 2013; 2:e00924. [PubMed: 24192035]

Oka C, Nakano T, Wakeham A, de la Pompa JL, Mori C, Sakai T, Okazaki S, Kawaichi M, Shiota K, Mak TW, Honjo T. Disruption of the mouse RBP-J kappa gene results in early embryonic death. Development. 1995; 121:3291–3301. [PubMed: 7588063]

Okamura D, Maeda I, Taniguchi H, Tokitake Y, Ikeda M, Ozato K, Mise N, Abe K, Noce T, Izpisua Belmonte JC, Matsui Y. Cell cycle gene-specific control of transcription has a critical role in proliferation of primordial germ cells. Genes Dev. 2012; 26:2477–2482. [PubMed: 23154982]

Oldham MC, Langfelder P, Horvath S. Network methods for describing sample relationships in genomic datasets: application to Huntington's disease. BMC Syst Biol. 2012; 6:63. [PubMed: 22691535]

Parchem RJ, Ye J, Judson RL, LaRussa MF, Krishnakumar R, Blelloch A, Oldham MC, Blelloch R. Two miRNA clusters reveal alternative paths in late-stage reprogramming. Cell Stem Cell. 2014; 14:617–631. [PubMed: 24630794]

Park CY, Choi YS, McManus MT. Analysis of microRNA knockouts in mice. Hum Mol Genet. 2010; 19(R2):R169–R175. [PubMed: 20805106]

Patterson M, Gaeta X, Loo K, Edwards M, Smale S, Cinkornpumin J, Xie Y, Listgarten J, Azghadi S, Douglass SM, et al. let-7 miRNAs can act through notch to regulate human gliogenesis. Stem Cell Reports. 2014; 3:758–773. [PubMed: 25316189]

Pernaute B, Spruce T, Smith KM, Sánchez-Nieto JM, Manzanares M, Cobb B, Rodríguez TA. MicroRNAs control the apoptotic threshold in primed pluripotent stem cells through regulation of BIM. Genes Dev. 2014; 28:1873–1878. [PubMed: 25184675]

Qi J, Yu JY, Shcherbata HR, Mathieu J, Wang AJ, Seal S, Zhou W, Stadler BM, Bourgin D, Wang L, et al. microRNAs regulate human embryonic stem cell division. Cell Cycle. 2009; 8:3729–3741. [PubMed: 19823043]

Qian X, Goderie SK, Shen Q, Stern JH, Temple S. Intrinsic programs of patterned cell lineages in isolated vertebrate CNS ventricular zone cells. Development. 1998; 125:3143–3152. [PubMed: 9671587]

Reinhart BJ, Slack FJ, Basson M, Pasquinelli AE, Bettinger JC, Rougvie AE, Horvitz HR, Ruvkun G. The 21-nucleotide let-7 RNA regulates developmental timing in Caenorhabditis elegans. Nature. 2000; 403:901–906. [PubMed: 10706289]

Rosa A, Spagnoli FM, Brivanlou AH. The miR-430/427/302 family controls mesendodermal fate specification via species-specific target selection. Dev Cell. 2009; 16:517–527. [PubMed: 19386261]

Seong Y, Lim DH, Kim A, Seo JH, Lee YS, Song H, Kwon YS. Global identification of target recognition and cleavage by the Microprocessor in human ES cells. Nucleic Acids Res. 2014; 42:12806–12821. [PubMed: 25326327]

Shi R, Chiang VL. Facile means for quantifying microRNA expression by real-time PCR. Biotechniques. 2005; 39:519–525. [PubMed: 16235564]

Stadler B, Ivanovska I, Mehta K, Song S, Nelson A, Tan Y, Mathieu J, Darby C, Blau CA, Ware C, et al. Characterization of microRNAs involved in embryonic stem cell states. Stem Cells Dev. 2010; 19:935–950. [PubMed: 20128659]

Suh MR, Lee Y, Kim JY, Kim SK, Moon SH, Lee JY, Cha KY, Chung HM, Yoon HS, Moon SY, et al. Human embryonic stem cells express a unique set of microRNAs. Dev Biol. 2004; 270:488–498. [PubMed: 15183728]

Tang F, Kaneda M, O'Carroll D, Hajkova P, Barton SC, Sun YA, Lee C, Tarakhovsky A, Lao K, Surani MA. Maternal microRNAs are essential for mouse zygotic development. Genes Dev. 2007; 21:644–648. [PubMed: 17369397]

Tian Y, Liu Y, Wang T, Zhou N, Kong J, Chen L, Snitow M, Morley M, Li D, Petrenko N, et al. A microRNA-Hippo pathway that promotes cardiomyocyte proliferation and cardiac regeneration in mice. Sci Transl Med. 2015; 7:279ra38.

Ventura A, Young AG, Winslow MM, Lintault L, Meissner A, Erkeland SJ, Newman J, Bronson RT, Crowley D, Stone JR, et al. Targeted deletion reveals essential and overlapping functions of the miR-17 through 92 family of miRNA clusters. Cell. 2008; 132:875–886. [PubMed: 18329372]

Vidigal JA, Ventura A. The biological functions of miRNAs: lessons from in vivo studies. Trends Cell Biol. 2015; 25:137–147. [PubMed: 25484347]

Wang Y, Medvid R, Melton C, Jaenisch R, Blelloch R. DGCR8 is essential for microRNA biogenesis and silencing of embryonic stem cell self-renewal. Nat Genet. 2007; 39:380–385. [PubMed: 17259983]

Wang Y, Baskerville S, Shenoy A, Babiarz JE, Baehner L, Blelloch R. Embryonic stem cell-specific microRNAs regulate the G1-S transition and promote rapid proliferation. Nat Genet. 2008; 40:1478–1483. [PubMed: 18978791]

Wang Y, Melton C, Li YP, Shenoy A, Zhang XX, Subramanyam D, Blelloch R. miR-294/miR-302 promotes proliferation, suppresses G1-S restriction point, and inhibits ESC differentiation through separable mechanisms. Cell Rep. 2013; 4:99–109. [PubMed: 23831024]

Zheng GX, Ravi A, Calabrese JM, Medeiros LA, Kirak O, Dennis LM, Jaenisch R, Burge CB, Sharp PA. A latent pro-survival function for the mir-290-295 cluster in mouse embryonic stem cells. PLoS Genet. 2011; 7:e1002054. [PubMed: 21573140]

Zhong W, Jiang MM, Schonemann MD, Meneses JJ, Pedersen RA, Jan LY, Jan YN. Mouse numb is an essential gene involved in cortical neurogenesis. Proc Natl Acad Sci U S A. 2000; 97:6844–6849. [PubMed: 10841580]

Highlights

- miR-302 is required for neural tube closure and embryonic survival
- miR-302 loss results in increased proliferation of neural progenitors
- miR-302 loss leads to precocious neuronal differentiation
- miR-290 and miR-302 act redundantly early in development

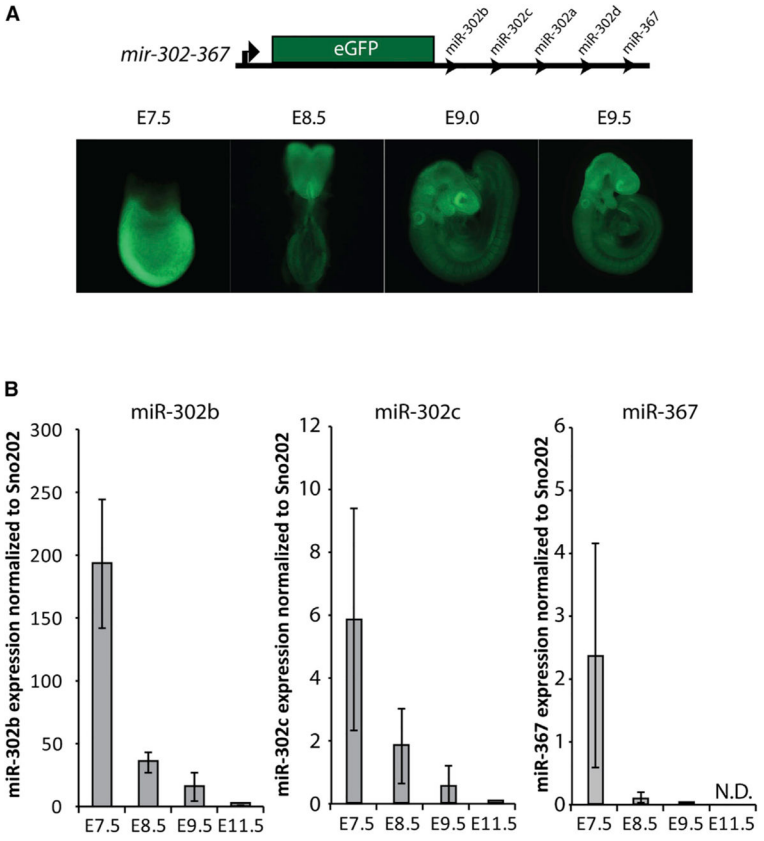

Figure 1. Expression of miR-302 during Embryonic Development

(A) Design of *mir-302* reporter with GFP expression from targeted *mir-302* locus. Reporter embryos show embryonic expression of *mir-302-GFP* at E7.5 and increased fluorescence in anterior neural structures from E8.5-E9.5.

(B) qRT-PCR of miR-302b, miR-302c, and miR-367 expression relative to sno202 (n = 3) at various developmental time points. Samples for E7.5 were whole embryos (extra-embryonic tissues were removed); cranial neural tissue was isolated at other time points. Error bars represent SD.

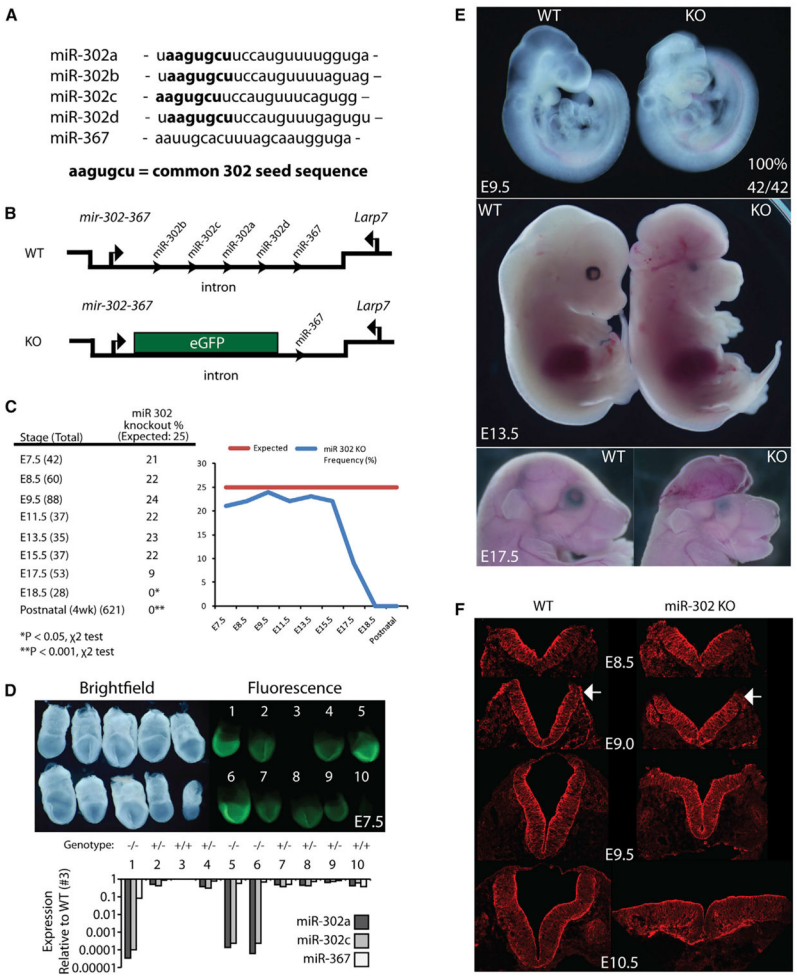

Figure 2. Deletion of *mir-302* Leads to Failure of Cranial Neural Tube Closure

(A) Sequences of mature miRNAs produced from the miR-302-367 cluster with common seed sequence for miR-302 miRNAs in bold. The seed sequence for miR-302c is shifted by one nucleotide relative to the other family members.

(B) Schematic showing design of knockout approach. EGFP coding sequence replaced the *mir-302a-d* hairpin sequences, leaving *mir-367* and *Larp7* sequences unaltered.

(C) Number of knockout embryos recovered at indicated developmental stages. Graph of observed knockout frequency showing reduced recovery after E15.5.

(D) Bright-field and fluorescent image of E7.5 litter from *mir-302* heterozygous intercross. Individual embryos were genotyped and assayed for expression of miR-302a, miR-302b, miR-367, and sno202. Normalized expression is relative to wild-type embryo #3.

(E) Bright-field images comparing wild-type and knockout embryos at indicated developmental stages. One hundred percent of *mir-302*-knockout embryos exhibited defects in mid/hindbrain closure at E9.5 (n = 42 mutants).

(F) Transverse hindbrain sections of wild-type and knockout embryos with immunohistochemistry staining using a pan-cadherin antibody at indicated developmental stages. Arrows indicate area of dorsolateral bending.

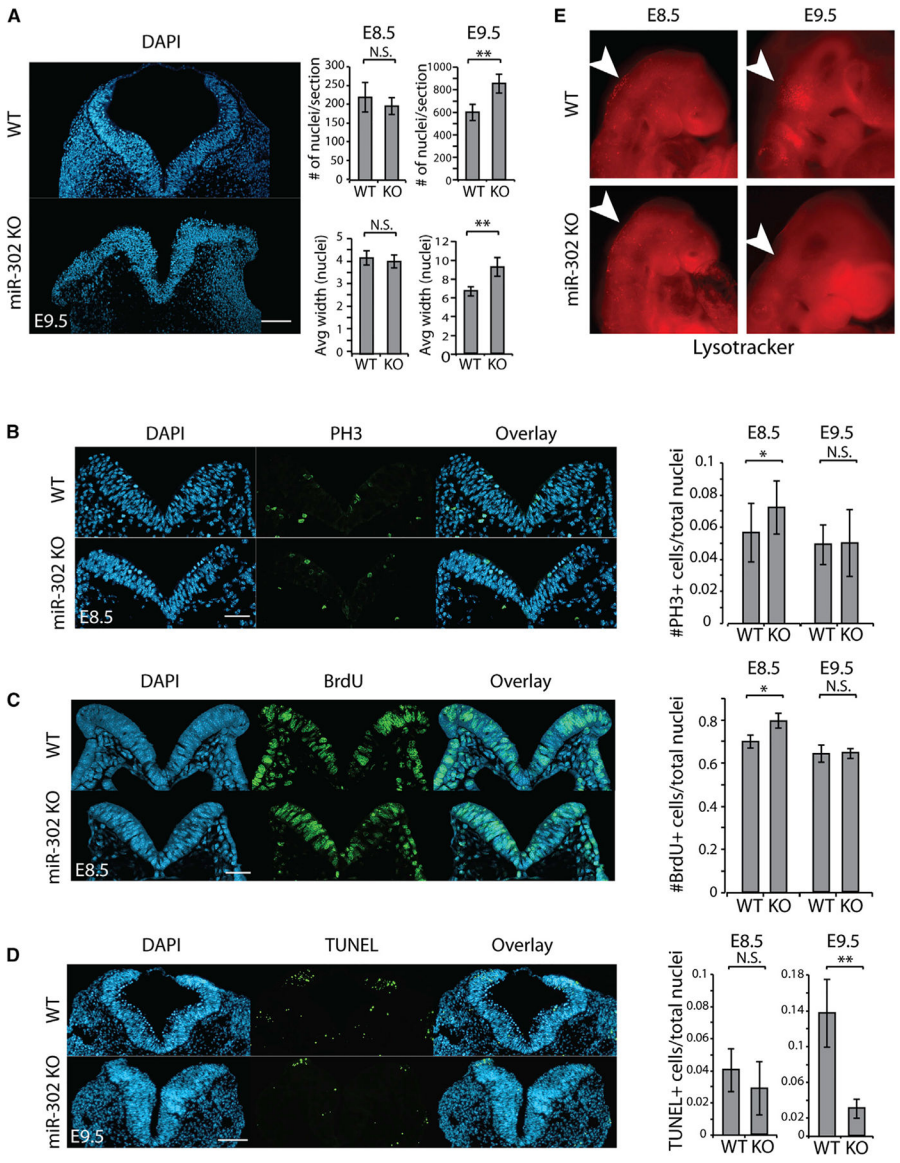

Figure 3. Increased Thickness of Neuroepithelium in *mir-302*-Knockout Embryos

(A) Transverse sections through wild-type and mutant embryonic hindbrain at E9.5 stained for DAPI to enable counting of nuclei (n = 3 embryos, six sections per embryo). Quantification at E8.5 and E9.5. Error bars represent SD. *p < 0.05, **p < 0.005. The scale bar represents 100 μm.

(B) Immunohistochemistry against PH3 to visualize cells in M phase of the cell cycle. Quantification of PH3-positive cells was calculated as the percentage of PH3-positive cells out of total (DAPI+) neuroepithelial cells at indicated developmental stages. Error bars represent SD (n = 3 embryos, six sections per embryo). *p < 0.05, **p < 0.005. The scale bar represents 50 μm.

(C) BrdU incorporation analysis after 2 hr pulse. Quantification of BrdU-positive cells was calculated as the percentage of BrdU-positive cells out of total neuroepithelial cells at

indicated developmental stages. Error bars represent SD (n = 3 embryos, six sections per embryo). *p < 0.05, **p < 0.005. The scale bar represents 50 μm.

(D) TUNEL assay was used to identify apoptotic cells in transverse sections of presumptive hindbrain. Quantification of TUNEL-positive cells was calculated as the percentage of TUNEL-positive cells out of total neuroepithelial cells at indicated developmental stages. Error bars represent SD (n = 3 embryos, six sections per embryo). *p < 0.05, **p < 0.005. The scale bar represents 100 μm.

(E) LysoTracker staining labels dead cells. White arrows point to comparable regions of mutant and wild-type embryos. A qualitative decrease in LysoTracker staining was observed at E9.5 (n = 3). Differences in staining were less pronounced at E8.5 between wild-type and knockout.

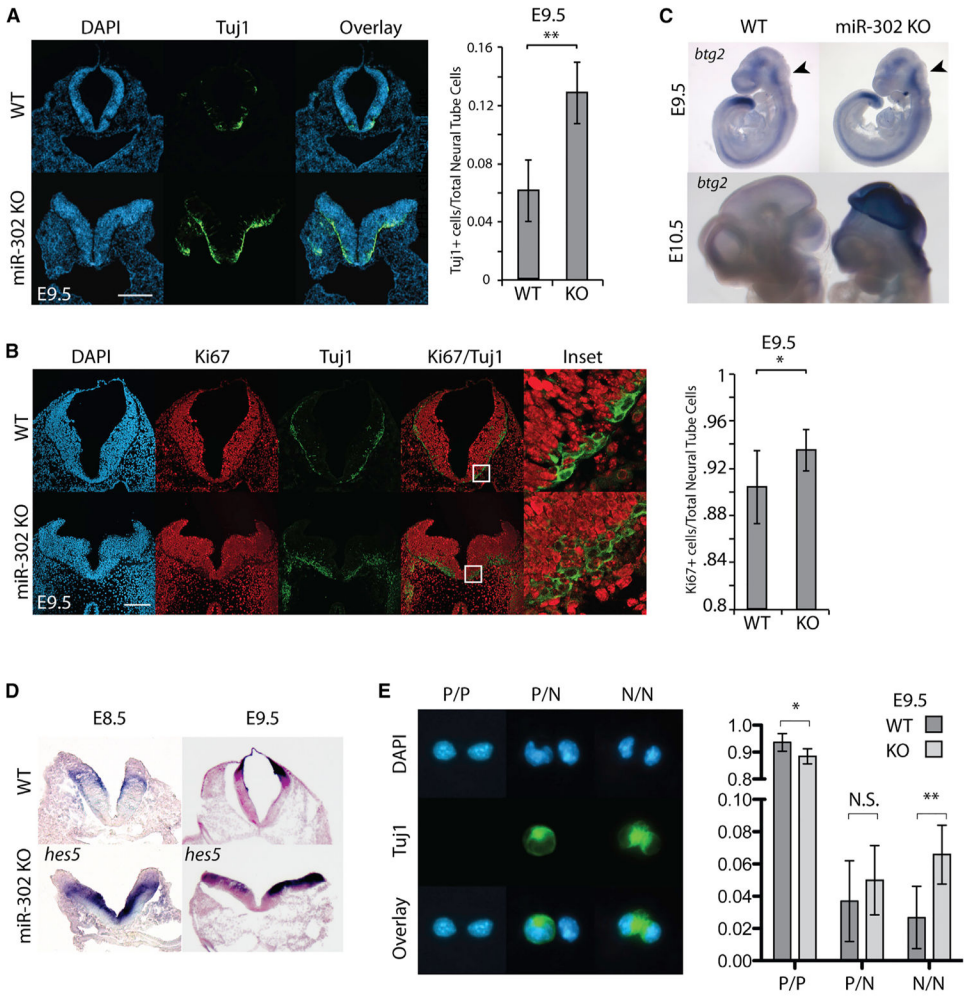

Figure 4. Precocious Neural Differentiation in *mir-302*-Knockout Embryos

(A) Tuj1 immunohistochemistry to visualize β-III-tubulin+ post-mitotic neural cells. Quantification of Tuj1+ cells was calculated as the percentage of Tuj1+ cells out of total neuroepithelial cells (DAPI+) at E9.5. Error bars represent SD (n = 3 embryos, six sections/embryo). *p < 0.05, **p < 0.005. The scale bar represents 200 μm.

(B) Immunohistochemistry against Ki67 was used to identify cycling cells, and Tuj1 was used to identify neurons. Quantification of Ki67+ cells was calculated as the percentage of Ki67+ cells out of total neuroepithelial cells at E9.5. Error bars represent SD (n = 3 embryos, six sections per embryo). *p < 0.05, **p < 0.005. Increased Ki67+ staining and increased Tuj1+ staining in the knockout is due to a greater number of Ki67+ cells that are also Tuj1+. The scale bar represents 100 μm.

(C) In situ hybridization using probe against *Btg2* to identify neurogenic dividing cells.

(D) In situ hybridization using probe against *Hes5* to identify neural progenitors. Transverse sections of embryonic hindbrain counterstained with Fast Red.

(E) Individual neuroepithelial cells were plated at clonal density, incubated for 24 hr, fixed, then stained for Tuj1. Pairs of cells that were generated from a single precursor were scored

for three possible division types. Quantification represents the average of >150 cells per embryo and genotype (n = 3 embryos). *p < 0.05, **p < 0.005.

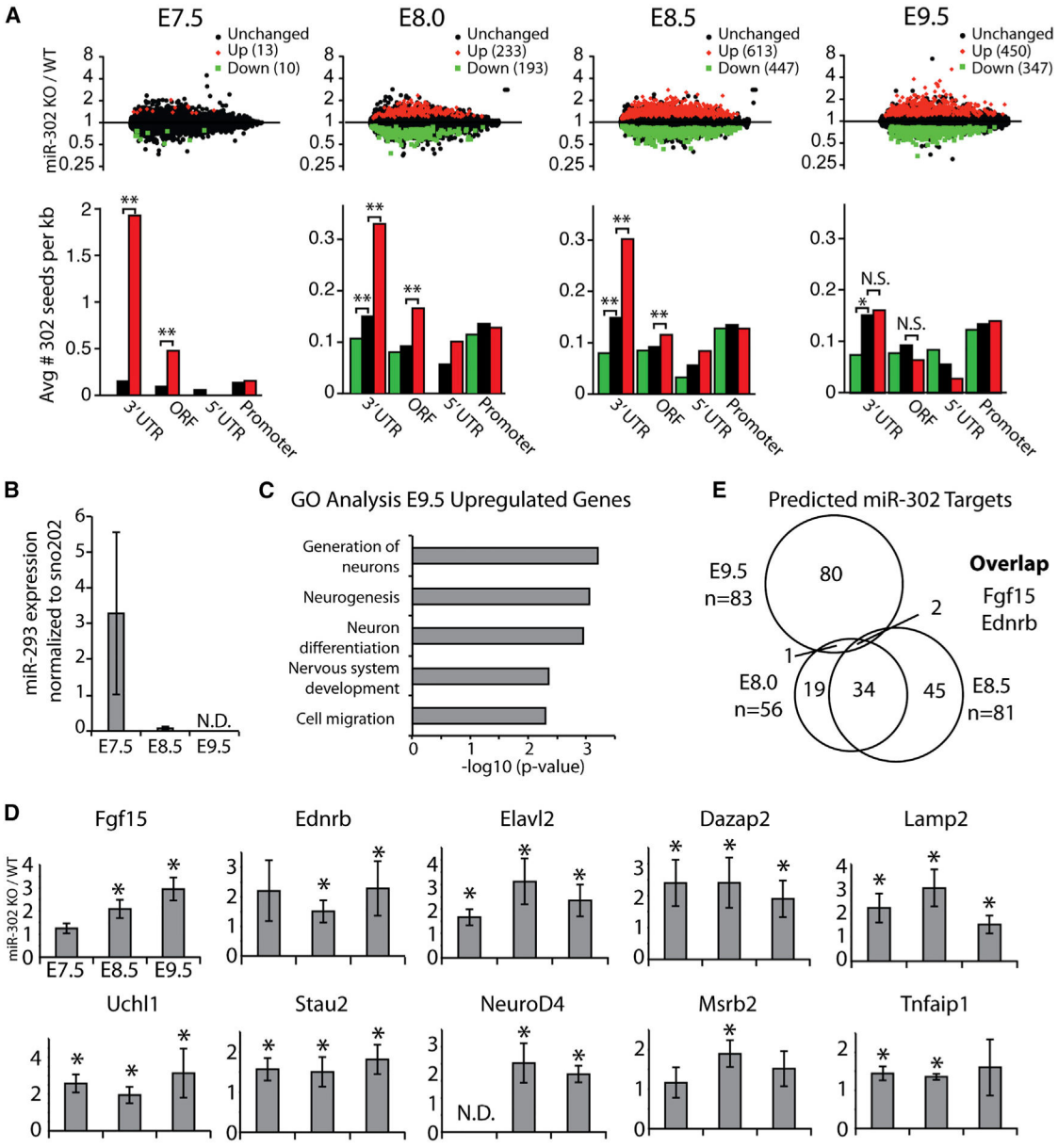

Figure 5. Identification of miR-302 Targets

(A) Microarray analysis of wild-type and knockout embryos at E7.5, E8.0, E8.5, and E9.5. Significantly upregulated transcripts are shown as red diamonds, downregulated transcripts as green squares, and unchanged transcripts as black circles (adjusted p value < 0.05, p < 0.1 for E7.5) (n = 3 embryos at each developmental time point). Analysis of seed matches in the promoter, 5′UTR, ORF, and 3′UTR of downregulated and upregulated transcripts. Data are presented as the mean number of seeds matches per kilobase of sequence for the listed groups of altered genes described in (A). p values calculated by the Wilcoxon rank sum test and Bonferroni corrected are shown for p < 0.01. *p < 0.05, **p < 0.005.

(B) qRT-PCR of miR-293 expression relative to sno202 (n = 3) at various developmental time points. Samples for E7.5 were whole embryos; at other time points, cranial neural tissue (i.e., neuroepithelium/neural tube) was isolated. Error bars represent SD.
(C) Gene Ontology analysis of upregulated genes in knockout embryos at E9.5 reveals enrichment for neural development-related terms.
(D) qRT-PCR of ten predicted targets that were upregulated in microarray analysis. Expression was normalized to *Rpl7* (n = 3 embryos for each genotype and developmental stage). *$p < 0.05$.
(E) Venn diagram showing the overlap of genes that are upregulated at E8.0, E8.5, and E9.5. *Fgf15* and *Ednrb* were the only two genes upregulated across all time points.

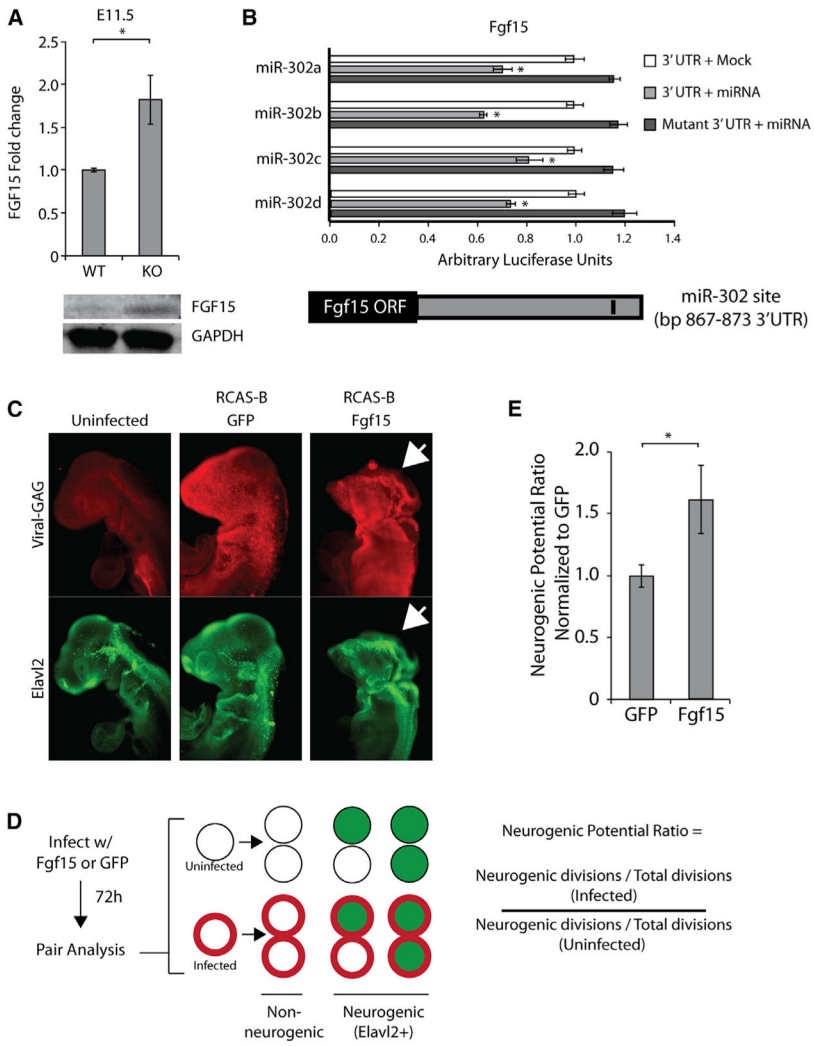

Figure 6. *Fgf15* Promotes Neural Differentiation and Is a Direct Target of miR-302

(A) Western blot assaying levels of FGF15 in wild-type versus knockout brain at E11.5. Quantification represents average expression relative to wild-type (n = 3). *p < 0.05.

(B) Luciferase reporter assay verifying miRNA-mediated translational repression of *Fgf15*. Luciferase activity in cells transfected with reporters expressing either wild-type or mutant UTRs with or without co-transfection of indicated miRNAs normalized to transfection with control miRNA (mock) (n = 3 technical replicates). *p < 0.05. Schematic of *Fgf15* mRNA with miR-302 binding site indicated in the 3′ UTR.

(C) Whole-mount immunohistochemistry against GAG and Elavl2 in chicken embryos 72 hr post-infection of the neuroepithelium.

(D) Pair analysis was performed on cranial neuroepithelium 72 hr after infection. Pairs were grouped into GAG-positive and GAG-negative to compare neural differentiation associated with viral overexpression of *Fgf15* or GFP. Neurogenic division ratio is calculated as the ratio of divisions giving rise to neurogenic (Elavl2+) progeny versus non-neurogenic progeny in GAG+ versus GAG− divisions (n = 3 embryos).

(E) Average neurogenic potential ratio of *Fgf15* and GFP infected neural cells (n = 3 embryos). *p < 0.05.

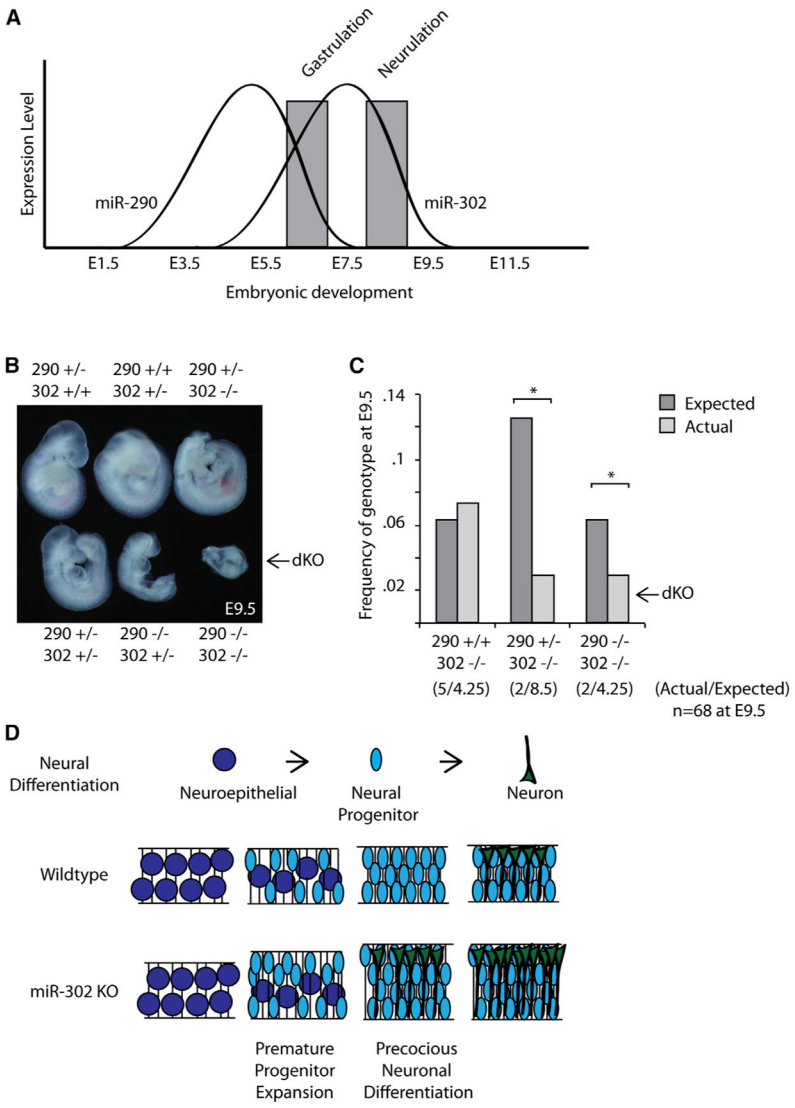

Figure 7. *mir-290* and *mir-302* Are Functionally Redundant

(A) Schematic summary of embryonic expression of *mir-290* and *mir-302* showing an overlapping expression pattern during early development.

(B) Bright-field images of embryos recovered at E9.5 with genotypes listed. Loss of three alleles corresponding to *mir-290* and *mir-302* results in early embryonic death and severe phenotypic embryos.

(C) Recovery of *mir-302* knockout embryos at E9.5 is lost when one or two alleles of *mir-290* are deleted. Expected number of recovered embryos indicated relative to expected. *$p < 0.05$.

(D) Schematic summary of the *mir-302* phenotype.